Phosphine and Phosphite Complexes of a Coordinatively Unsaturated Triplatinum Hydride: Structure of $[Pt_3(\mu_3\text{-}H)(\mu\text{-}Ph_2PCH_2PPh_2)_3\{P(OMe)_3\}]PF_6$

Ravindranath Ramachandran, Dong-Sheng Yang, Nicholas C. Payne, and Richard J. Puddephatt*

Department of Chemistry, University of Western Ontario, London, Ontario, Canada N6A 5B7

Received April 6, 1992

The coordinatively unsaturated cluster $[Pt_3(\mu_3\text{-}H)(\mu\text{-dppm})_3]^+$ adds phosphine or phosphite ligands L to give $[Pt_3(\mu_3\text{-}H)L(\mu\text{-dppm})_3]^+$ (**5**). The structure of (**5a**)PF_6, where L = $P(OMe)_3$, was determined by X-ray diffraction techniques [space group $P\bar{1}$, a = 14.083 (3) Å, b = 25.755 (3) Å, c = 11.609 (2) Å, α = 91.19 (1)°, β = 112.39 (2)°, γ = 90.36 (1)°, R = 0.045, R_w = 0.056]. Combined information from the structure determination and low-temperature NMR studies shows that the ligand L is terminally bonded, that the $Pt_3(\mu_3\text{-}H)$ group is distorted such that the hydride binds most strongly to the platinum atom having the higher coordination number and that the ligand L can migrate very easily around the Pt_3 triangle. A theoretical rationalization of the observed structure is given based on EHMO calculations.

Introduction

The role of both steric and electronic effects of tertiary phosphine and phosphite ligands on the chemistry of platinum cluster complexes is well documented.[1-8] For example, it has been shown that some phosphine ligands, L, add reversibly to the 42-electron clusters $[Pt_3(\mu\text{-}CO)_3L_3]$ to give $[Pt_3(\mu\text{-}CO)_3L_4]$, and this can lead to either ligand substitution reactions or to cluster fragmentation.[2,7,8] Similarly, the 42-electron cluster $[Pt_3(\mu\text{-}CO)(\mu\text{-dppm})_3]^{2+}$ (**1**); dppm = $Ph_2PCH_2PPh_2$)[9] reacts with phosphine and phosphite ligands, L, to give $[Pt_3(\mu\text{-}CO)(\mu\text{-dppm})_3L]^{2+}$ (**2**).[10] In these complexes (**2**), the carbonyl ligand is asymmetrically bridging the triplatinum center, being most strongly bound to the platinum center with highest coordination number.[10] Similarly, in the 46-electron triplatinum complex $[Pt_3(\mu\text{-}CO)(\mu\text{-dmpm})_4]^{2+}$ (**3**), the carbonyl ligand is bonded most strongly to the two platinum atoms which have the extra phosphine donor to the extent that it is considered to be present as a μ_2-CO ligand.[11] Evans has suggested, based on extended Huckel molecular orbital calculations (EHMO), that, in these complexes, the capping carbonyl acts primarily as a π-acid ligand and hence binds more strongly to the metal centers with greater electron density.[12] The nature of the carbonyl distortion in both **2** and **3** follows naturally from this theory. It was therefore of interest to study the reactivity of phosphine and phosphite ligands with the hydridotriplatinum complex $[Pt_3(\mu_3\text{-}H)(\mu\text{-dppm})_3]^+$ (**4**), which has a capping hydride ligand.[13-16] Since the hydride ligand can have no π-acid character, significant differences might be expected from the analogous reactions of the carbonyl cluster **1** if the π-acid theory is correct. The results of this study are given below, and a preliminary account has been published.[16]

Experimental Section

NMR spectra were recorded by using Varian XL200 or XL300 spectrometers. Complex **4** was prepared by the literature method.[13]

$[Pt_3(\mu_3\text{-}H)(\mu\text{-dppm})_3\{P(OMe)_3\}]PF_6\cdot 0.5CH_2Cl_2$ [(5a)$PF_6\cdot 0.5CH_2Cl_2$]. To a solution of $[Pt_3(\mu_3\text{-}H)(\mu\text{-dppm})_3]PF_6$ (40 mg) in CH_2Cl_2 (10 mL) was added $P(OMe)_3$ (2.5 μL) by syringe. The contents were stirred under nitrogen for 20 min. The solvent was evaporated under vacuum to give the product **5a**, which was recrystallized from CH_2Cl_2/pentane as red crystals. The reaction was essentially quantitative as monitored by ^{31}P NMR spectroscopy, and the isolated yield was ~85%. Anal. Calcd for $C_{78.5}H_{77}ClF_6O_3P_8Pt_3$: C, 46.0; H, 3.8. Found: C, 46.0; H, 3.8.

In a similar manner was prepared $[Pt_3(\mu_3\text{-}H)(\mu\text{-dppm})_3\{P(OEt)_3\}]PF_6$ [(**5b**)PF_6]. Anal. Calcd for $C_{81}H_{82}F_6O_3P_8Pt_3$: C, 47.5; H, 4.0. Found: C, 47.3; H, 4.1. $[Pt_3(\mu_3\text{-}H)(\mu\text{-dppm})_3\{P(OPh)_3\}]PF_6$ [(**5c**)PF_6] Anal. Calcd for $C_{93}H_{82}F_6O_3P_8Pt_3$: C, 50.9; H, 3.8. Found: C, 50.6; H, 4.0. $[Pt_3(\mu_3\text{-}H)(\mu\text{-dppm})_3(PMePh_2)]PF_6$ [(**5d**)PF_6] Anal. Calcd for $C_{88}H_{80}F_6P_8Pt_3$: C, 50.7; H, 3.9. Found: C, 50.2; H, 3.7.

X-ray Structure Analysis. Red crystals of $[Pt_3(\mu_3\text{-}H)(\mu\text{-dppm})_3\{P(OMe)_3\}]PF_6\cdot 0.5CH_2Cl_2$ [(**5a**)$PF_6\cdot 0.5CH_2Cl_2$] were grown from CH_2Cl_2/pentane. A photographic examination showed triclinic symmetry and established the space group $P\bar{1}$, No. 2.[17] The crystal density was determined by neutral buoyancy in a mixture of $CHBr_3$/hexane. The cell constants and orientation matrix were refined by using the angular settings for 20 high-angle reflections on an Enraf-Nonius CAD4F diffractometer.[18] ω-Scans of intense, low-angle reflections were recorded.

(1) (a) Albinati, A. *Inorg. Chim. Acta* **1977**, *22*, L3. (b) Albinati, A.; Carturan, G.; Musco, A. *Inorg. Chim. Acta* **1976**, *16*, L3.
(2) Chatt, J.; Chini, P. *J. Chem. Soc. A* **1970**, 1538.
(3) Vranka, R. G.; Dahl, L. F.; Chini, P.; Chatt, J. *J. Am. Chem. Soc.* **1969**, *91*, 1574.
(4) Moor, A.; Pregosin, P. S.; Venanzi, L. M.; Welch, A. J. *Inorg. Chim. Acta* **1984**, *85*, 103.
(5) (a) Barbier, J. P.; Bender, R.; Braunstein, P.; Fischer, J.; Ricard, L. *J. Chem. Res., Synop.* **1978**, 230; *J. Chem. Res., Miniprint* **1978**, 2913. (b) Bender, R.; Braunstein, P.; Fischer, J.; Ricard, L.; Mitscher, A. *Nouv. J. Chim.* **1981**, *5*, 81.
(6) Evans, D. G.; Hallam, M. F.; Mingos, D. M. P.; Wardle, W. M. *J. Chem. Soc., Dalton Trans.* **1987**, 1889.
(7) (a) Mingos, D. M. P.; Wardle, W. M. *Transition Met. Chem. (Weinheim, Ger.)* **1985**, *10*, 441. (b) Ermenko, N. K.; Mednikov, E. G.; Kurasov, S. S. *Russ. Chem. Rev. (Engl. Transl.)* **1985**, *54*, 394.
(8) (a) Browning, C. S.; Farrar, D. H.; Gukathasan, R. R.; Morris, S. A. *Organometallics* **1985**, *4*, 1750. (b) Mingos, D. M. P.; Williams, I. D.; Watson, M. J. *J. Chem. Soc., Dalton Trans.* **1988**, 1509.
(9) (a) Ferguson, G.; Lloyd, B. R.; Puddephatt, R. J. *Organometallics* **1986**, *5*, 344. (b) Puddephatt, R. J.; Manojlovic-Muir, Lj.; Muir, K. W. *Polyhedron* **1990**, *9*, 2767.
(10) (a) Bradford, A. M.; Jennings, M. C.; Puddephatt, R. J. *Organometallics* **1988**, *7*, 792. (b) Bradford, A. M.; Douglas, G.; Manojlovic-Muir, Lj.; Muir, K. W.; Puddephatt, R. J. *Organometallics*.
(11) Ling, S. S. M.; Hadj-Bagheri, N.; Manojlovic-Muir, Lj.; Muir, K. W.; Puddephatt, R. J. *Inorg. Chem.* **1987**, *26*, 231.
(12) Evans, D. G. *J. Organomet. Chem.* **1988**, *352*, 397.
(13) Lloyd, B. R.; Pudephatt, R. J. *J. Am. Chem. Soc.* **1987**, *109*, 7785.
(14) (a) Ferguson, G.; Lloyd, B. R.; Manojlovic-Muir, Lj.; Muir, K. W.; Puddephatt, R. J. *Inorg. Chem.* **1986**, *25*, 4190. (b) Jennings, M. C.; Puddephatt, R. J. *Inorg. Chem.* **1988**, *27*, 4280. (c) Jennings, M. C.; Manojlovic-Muir, Lj.; Muir, K. W.; Puddephatt, R. J. *J. Chem. Soc., Chem. Commun.* **1989**. (d) Payne, N. C.; Ramachandran, R.; Schoettel, G.; Vittal, J. J.; Puddephatt, R. J. *Inorg. Chem.* **1991**, *30*, 4048.
(15) (a) Mealli, C. *J. Am. Chem. Soc.* **1985**, *107*, 2245. (b) Summerville, R. H.; Hoffmann, R. *J. Am. Chem. Soc.* **1978**, *98*, 7240. (c) Underwood, D.; Hoffmann, R.; Tatsumi, T.; Nakamura, A.; Yamamoto, Y. *J. Am. Chem. Soc.* **1985**, *107*, 5968.
(16) Ramachandran, R.; Yang, D.-S.; Payne, N. C.; Puddephatt, R. J. *Inorg. Chim. Acta* **1991**, *186*, 1.
(17) *International Tables for X-ray Crystallography*; Kynoch Press: Birmingham, England: 1969, Vol I; 1974, Vol IV.
(18) *Enraf-Nonius CAD4F Users Manual*; Enraf-Nonius Delft: Delft, The Netherlands, 1984.

0020-1669/92/1331-4236$03.00/0

Table I. Summary of X-ray Structure Determination of Complex **5a**

compd; fw	$C_{78.5}H_{77}Cl_1F_6O_3P_8Pt_3$; 2050.97
cryst syst; space group	triclinic; $P\bar{1}$ (No. 2)
cell dimens (Å; deg)	a = 14.083 (3); α = 91.91 (1) b = 25.755 (3); β = 112.39 (2) c = 11.609 (2); γ = 90.36 (1)
cell vol (Å^3); Z	3892 (2); 2
temp, °C	23
density, g cm^{-3}: obsd; calcd	1.791 (2); 1.750
radiation, wavelength (Å)	Mo, λ(Kα mean) 0.710 73
approx cryst dimens (mm)	0.28 × 0.20 × 0.59
no. of data; std collcd	11198; 448
abs coeff (cm^{-1})	56.90
no. of unique data; signif	9529; $I > 0$
no. of observns; no. of variables	7581; 326
final model: R; R_w[a]	0.045; 0.056

[a] $R = \sum\|\|F_o\| - \|F_c\|\|/\sum\|F_o\|$; $R_w = [\sum w(\|F_o\| - \|F_c\|)^2/\sum w(F_o)^2]^{1/2}$.

Intensity data were measured with variable scan speeds within a maximum time per datum of 60 s; background estimates were made by extending the scan by 25% on each side. Standard reflections were monitored regularly and showed decay averaging 3.4%. In all, 11 198 data were recorded, of which 448 were standards. The data were processed using the Enraf-Nonius Structure Determination Package,[19] Version 3.0, running on a PDP 11/23+ computer. Standard deviations were assigned based on counting statistics,[19] and decay and absorption corrections (program AGNOST[20]) were applied. After symmetry-equivalent data were averaged (926 observations, R_{av} on F = 0.021), 9529 unique data with $I > 0$ were available for the analysis. Crystal data and experimental conditions are summarized in Table I.

The structure was solved by Patterson and Fourier techniques, and refined by full-matrix least-squares techniques on F, minimizing the function $\sum w(\|F_o\| - \|F_c\|)^2$, where the weight w is given by $1/[\{\sigma(F)\}^2 + 0.000281F^2]$. Scattering factors for neutral non-hydrogen atoms and the real parts of the anomalous dispersion correction were taken from ref 17, while H atom scattering factors were taken from ref 21. Once all the non-hydrogen atoms were located, refinement of the structure was completed by use of the SHELX-76 program.[22] The 12 phenyl rings were constrained to D_{6h} symmetry (C–C = 1.392 Å) and refined with individual thermal parameters for the ring carbon atoms. At a stage of refinement, a difference Fourier map showed disorder in the $P(OMe)_3$ ligand with site occupancy factor 75:25. The geometry of the disordered $P(OMe)_3$ units were constrained at P–O = 1.60 Å, O–C = 1.43 Å, and P···C = 2.625 Å. Refinement continued with a single overall temperature factor for the oxygen and carbon atoms of the $P(OMe)_3$ group. A difference Fourier synthesis run at this stage showed the presence of 0.5 CH_2Cl_2 in the asymmetric unit of the cell. One of the two PF_6^- anions in the unit cell occupies a special position [P(8), Wyckoff *f*, site symmetry $\bar{1}$, multiplicity 1]. The remaining anion shares a special position with the dichloromethane solvent molecule [P(9) and C(9), Wyckoff *h*, site symmetry $\bar{1}$, multiplicity] in a disordered arrangement. The PF_6^- anions were refined as regular octahedra with P–F = 1.58 Å. Only the Pt, P, and F atoms were assigned anisotropic thermal parameters. The non-hydrogen atoms of the $P(9)F_6^-$ anion and the CH_2Cl_2 molecule were refined with a single overall temperature factor. All the hydrogen atoms, except those belonging to the $P(OMe)_3$ ligand, solvent and the hydride, were included in the structural model in calculated positions (sp^2 C–H = 0.90 Å; sp^3 C–H = 0.95 Å) with thermal parameters set at 110% of that of the atom to which they are bonded.

Final positional and thermal parameters for the non-hydrogen atoms are given in Table II, and selected bond distances and angles are in Table III. Additional experimental details and complete bond parameters, hydrogen atom parameters, anisotropic thermal parameters, selected torsional angles and weighted least-squares planes are given in Tables S1–S5 respectively.

EHMO Calculations. The dimensions used were averages obtained from the structure of **5a** and with d(Pt–H) = 1.85 Å. Parameters were from ref 15.

(19) *Enraf-Nonius Structure Determination Package, SDP-PLUS*, Version 3.0; Enraf-Nonius Delft: Delft, The Netherlands, 1984.
(20) de Meulenaer, J.; Tompa, H. *Acta Crystallogr.* **1965**, *19*, 1014.
(21) Stewart, R. F.; Davidson, E. R.; Simpson, W. T. *J. Chem. Phys.* **1965**, *42*, 3175.
(22) Sheldrick, G. M. *SHELX-76: A Program for Crystal Structure Determination*; Cambridge University Press: Cambridge, England, 1976.

Table II. Selected Atomic Positional (×10^4) and Thermal (×10^3) Parameters for **5a**

Atom	x	y	z	U or U_{eq} (Å^2)
Pt(1)	2449.7 (3)	3054.7 (2)	575.5 (4)	39.8 (2)
Pt(2)	2020.7 (3)	2064.3 (2)	690.8 (4)	40.1 (2)
Pt(3)	3969.6 (3)	2416.5 (2)	1298.9 (4)	43.1 (2)
P(1)	842 (2)	3379 (1)	−117 (3)	43 (1)
P(2)	438 (2)	2242 (1)	−802 (3)	45 (1)
P(3)	2429 (2)	1183 (1)	825 (3)	47 (1)
P(4)	4628 (2)	1597 (1)	1409 (3)	48 (1)
P(5)	5181 (2)	3017 (1)	2314 (3)	48 (1)
P(6)	3526 (2)	3701 (1)	665 (3)	55 (1)
P(7)	2168 (3)	2169 (2)	2697 (3)	70 (2)
C(1)	−73 (8)	2838 (4)	−340 (10)	45 (3)
C(2)	3811 (8)	1121 (5)	1760 (11)	55 (3)
C(3)	4647 (9)	3684 (5)	2120 (11)	55 (3)
C(11)	331 (5)	3712 (3)	−1603 (8)	51 (3)
C(21)	565 (6)	3799 (3)	1004 (7)	44 (3)
C(31)	311 (5)	2389 (3)	−2397 (7)	47 (3)
C(41)	−656 (6)	1787 (3)	−1148 (7)	46 (3)
C(51)	2298 (6)	788 (3)	−559 (7)	55 (3)
C(61)	1777 (7)	760 (4)	1556 (7)	55 (3)
C(71)	5938 (7)	1430 (4)	2453 (8)	57 (3)
C(81)	4683 (6)	1383 (3)	−66 (8)	48 (3)
C(91)	6295 (6)	3095 (3)	1886 (7)	51 (3)
C(101)	5772 (7)	2964 (3)	4010 (9)	55 (3)
C(111)	4026 (7)	3659 (4)	−553 (9)	65 (4)
C(121)	3102 (7)	4375 (4)	631 (8)	68 (4)
O(1)A	2326 (9)	2677 (4)	3571 (11)	108 (2)
O(2)A	2995 (8)	1776 (5)	3563 (11)	108 (2)
O(3)A	1198 (7)	2065 (5)	3064 (11)	108 (2)
C(4)A	3239 (13)	2988 (6)	3888 (23)	108 (2)
C(5)A	3030 (15)	1672 (9)	4784 (12)	108 (2)
C(6)A	402 (9)	1710 (8)	2331 (19)	108 (2)
O(1)B	3099 (17)	2533 (11)	3572 (34)	108 (2)
O(2)B	2658 (29)	1680 (10)	3535 (34)	108 (2)
O(3)B	1121 (18)	2298 (12)	2894 (42)	108 (2)
C(4)B	2937 (38)	3072 (12)	3734 (70)	108 (2)
C(5)B	3449 (4)	1759 (22)	4748 (38)	108 (2)
C(6)B	270 (27)	1869 (21)	2462 (63)	108 (2)

Table III. Selected Bond Distances (Å) and Angles (deg) for **5a**

Distances

Pt(3)–Pt(1)	2.592 (1)	Pt(1)–Pt(2)	2.635 (1)
Pt(3)–Pt(2)	2.705 (1)	Pt(1)–P(1)	2.266 (3)
Pt(2)–P(2)	2.298 (3)	Pt(2)–P(3)	2.339 (3)
Pt(3)–P(4)	2.297 (3)	Pt(3)–P(5)	2.248 (3)
Pt(1)–P(6)	2.217 (3)	Pt(2)–P(7)	2.268 (4)
P–CH_2	1.82 (1)–1.86 (1)	P–C(Ph)	1.81 (1)–1.84 (1)

Angles

Pt(3)–Pt(1)–Pt(2)	62.33 (2)	P(1)–Pt(1)–Pt(2)	99.82 (8)
Pt(3)–Pt(2)–Pt(1)	58.06 (2)	P(1)–Pt(1)–Pt(3)	162.14 (8)
Pt(2)–Pt(3)–Pt(1)	59.61 (2)	P(6)–Pt(1)–Pt(2)	152.15 (8)
P(6)–Pt(1)–Pt(3)	90.04 (9)	P(2)–Pt(2)–Pt(1)	85.60 (9)
P(2)–Pt(2)–Pt(3)	136.15 (9)	P(3)–Pt(2)–Pt(1)	152.87 (8)
P(3)–Pt(2)–Pt(3)	95.65 (8)	P(7)–Pt(2)–Pt(1)	91.45 (11)
P(7)–Pt(2)–Pt(3)	90.82 (11)	P(4)–Pt(3)–Pt(1)	151.64 (8)
P(4)–Pt(3)–Pt(2)	93.68 (8)	P(5)–Pt(3)–Pt(1)	95.94 (8)
P(5)–Pt(3)–Pt(2)	147.80 (8)	P(6)–Pt(1)–P(1)	107.7 (1)
P(3)–Pt(2)–P(2)	114.1 (1)	P(7)–Pt(2)–P(2)	115.8 (1)
P(7)–Pt(2)–P(3)	95.9 (1)	P(5)–Pt(3)–P(4)	112.4 (1)

Results

Formation of the Complexes $[Pt_3(\mu_3\text{-}H)(\mu\text{-dppm})_3L]PF_6$ [(5)-PF_6]. The reaction of $[Pt_3(\mu_3\text{-}H)(\mu\text{-dppm})_3]PF_6$ [(4)PF_6] with the phosphite ligands $P(OMe)_3$, $P(OEt)_3$, and $P(OPh)_3$ and the phosphine ligand $PMePh_2$ gave the corresponding complexes (**5a**)-PF_6, (**5b**)PF_6, (**5c**)PF_6, and (**5d**)PF_6, respectively in high yield according to eq 1. These complexes were thermally stable and could be isolated in analytically pure form as the red, crystalline hexafluorophosphate salts. Complex (**5a**)PF_6 was structurally characterized by a single-crystal X-ray diffraction study.

Structure of $[Pt_3(\mu_3\text{-}H)(\mu\text{-dppm})_3\{P(OMe)_3\}]PF_6\cdot0.5CH_2Cl_2$ [(5a)$PF_6\cdot0.5CH_2Cl_2$]. The structure of (**5a**)PF_6 determined by X-ray crystallographic methods, is comprised of discrete cations,

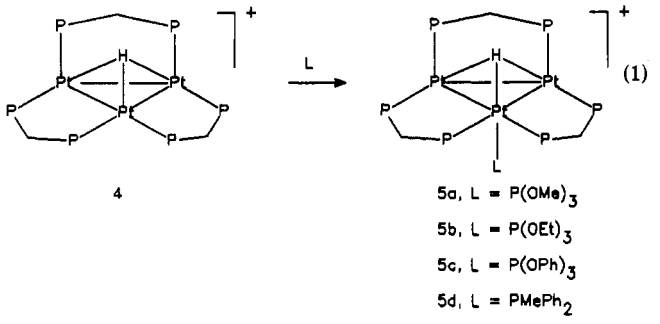

anions, and loosely entrapped dichloromethane as solvent of crystallization. The structure of the cation is characterized by bond lengths and bond angles given in Table III. Figure 1 shows the structure of the cation with one orientation of the disordered $P(OMe)_3$ ligand.

In the cation, the platinum atoms form a triangle with Pt–Pt distances of 2.592 (1), 2.635 (1), and 2.705 (1) Å and Pt–Pt–Pt angles of 58.06 (2), 59.61 (2), and 62.33 (2)°. The shortest of the three Pt–Pt bonds, Pt(1)–Pt(3) = 2.592 (1) Å, is associated with the platinum atoms which lack the terminal phosphite ligand. The triangle of Pt atoms is held together by three μ-dppm ligands, each of which bridges a Pt–Pt edge. Distortion from the ideal planar, latitudinal $Pt_3(\mu\text{-PCP})_3$ geometry is greatest at the Pt(2) center, whose coordination number is highest of the three platinum centers since it is bonded to the phosphite ligand. Thus the phosphorus atoms P(2) and P(3) lie 0.998 (3) and 0.291 (3) Å away from the Pt_3 plane, on the side opposite to that of $P(OMe)_3$ ligand. The Pt–P (dppm) bond lengths involving the Pt(2) from [2.339 (3), 2.298 (3) Å] are longer than those involving Pt(1) and Pt(3) [2.215 (3)–2.297 (3) Å]. These differences could be due either to steric or electronic effects associated with the higher coordination number at Pt(2). The $P(OMe)_3$ ligand is bound terminally to the Pt(2) atom and is perpendicular to the Pt_3 plane [P(7)–Pt(2)–Pt(1) = 91.45 (11)°, P(7)–Pt(2)–Pt(3) = 90.8 (1)°].

The Pt_2P_2C rings of the $Pt_2(\mu\text{-dppm})$ units adopt envelope conformations with the methylene carbon at the flap. All of the methylene carbon atoms C(1), C(2), and C(3) are directed toward the $P(OMe)_3$ ligand and are displaced from the Pt_3 plane by 0.08 (1), 0.19 (1), and 1.06 (1) Å, respectively. In this conformation of the $Pt_3(\mu\text{-dppm})_3$ unit, the phenyl rings are directed away from the bulkier, axial $P(OMe)_3$ ligand and the steric hindrance is thus minimized. The smaller hydride ligand is presumed to occupy the opposite face of the Pt_3 triangle, but it was not located in the X-ray study. Since a bridging hydride leads to lengthening of a metal–metal bond and the Pt–Pt bond lengths fall in the sequence Pt(2)–Pt(3) > Pt(1)–Pt(2) > Pt(1)–Pt(3), it is possible that the hydride ligand is associated mostly with the Pt(2)–Pt(3) bond.

Spectroscopic Characterization of Complexes 5a–d. The complexes **5** were fluxional in solution at room temperature, and hence NMR spectra were recorded at low temperature, typically at –90 °C in CD_2Cl_2 solution. At this temperature the fluxionality in these complexes was frozen out. The NMR labeling scheme is shown in Figure 2, the room-temperature ^1H and ^{31}P NMR spectral data are given in Table IV, and the low-temperature ^{31}P and ^{195}Pt NMR data are given in Table V.

The ^{31}P NMR spectra of **5a** at +20 and –90 °C are shown in Figure 2 and will be discussed in detail. The low-temperature ^{31}P NMR spectrum contains four signals in a 2:2:2:1 intensity ratio as expected. In these trinuclear $Pt_3(\mu\text{-dppm})_3$ complexes, the largest $J(PP)$ couplings are the translike couplings through the Pt–Pt bonds,[9-11] which in **5a** are $^3J(P^aP^c)$ and $^3J(P^bP^{b'})$. The observed spectrum contains two doublet resonances and a singlet resonance in the high-field region due to the phosphorus atoms of the bridging dppm ligands. The singlet at $\delta = -12.3$ [$^1J(PtP) = 2540$ Hz] is then readily assigned to P^b. The magnitude of

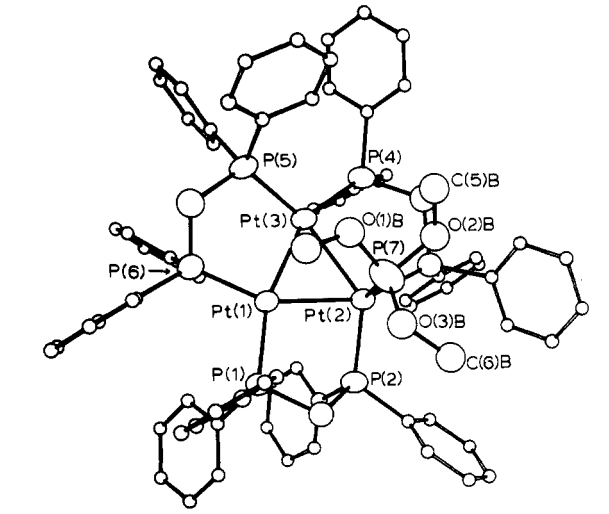

Figure 1. View of the structure of complex **5a**.

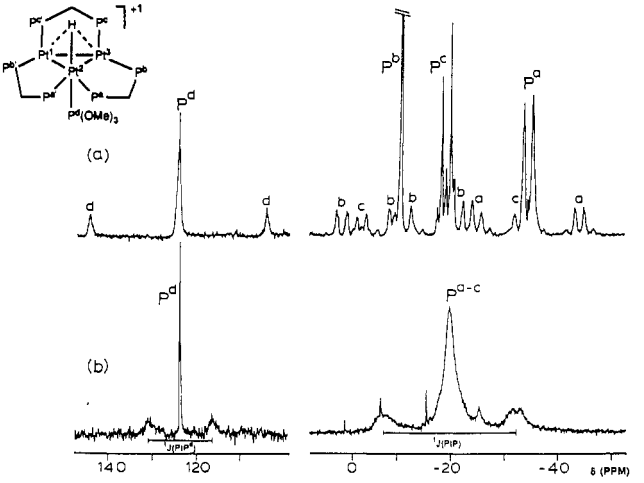

Figure 2. $^{31}P\{^1H\}$ NMR spectra of complex **5a**: (a) at –90 °C; (b) at +20 °C. Note the coalescence of dppm resonances and the much reduced magnitude of $^1J(PtP^d)$ in the +20 °C spectrum.

Table IV. ^1H and ^{31}P NMR Data for Complexes **5a–d** in CD_2Cl_2 at Room Temperature

	5a[a]	5b[b]	5c	5d[c]
δ(PtH)	–0.49	–0.59	–0.03	–0.96
^1J(PtH) (Hz)	590	570	551	
$^2J(P^dH)$ (Hz)	160	153	106	126
^2J(PH) (Hz)	7.5	7.5	9.5	
$\delta(CH^aH^b)$	5.93	6.16	5.88	5.80
$^3J(PtH^a)$ (Hz)	65	78	78	78
$^2J(H^aH^b)$ (Hz)	10		12	
$\delta(CH^aH^b)$	4.60	4.48	4.38	3.95
$\delta(P^{a-c})$	–21.6	–21.4	20.1[d]	–19.1
^1J(PtP) (Hz)	2980	2970	3140	2950
$\delta(P^d)$	123.6	117.3	95.1	–7.2
$^1J(PtP^d)$ (Hz)	1733	1650	2125	1200
$^2J(PtP^d)$ (Hz)	13	13.5	42	21

[a] δ(MeO) = 3.45; ^3J(PH) = 12 Hz. [b] δ(Me) = 1.00, $\delta(CH_2)$ = 3.87; ^3J(HH) = 7 Hz, ^3J(PH) = 7 Hz. [c] δ(Me) = 2.28. [d] ^2J(PtP) = 200 Hz, ^3J(PtP) = 18 Hz.

$^3J(P^bP^{b'})$ = 230 Hz can only be obtained from the ^{195}Pt satellite spectra. The resonances due to P^a [$\delta = -35.5$, $^3J(P^aP^c) = 190$ Hz, ^1J(PtP) = 2280 Hz] and P^c [$\delta = -20.6$, ^1J(PtP) = 3720 Hz] are assigned by correlation of ^1J(PtP) values with the Pt–P bond lengths and from a general trend that the ^{31}P chemical shifts move to high field when bound to platinum atoms with higher coordination number.[9-11] The resonance due to the $P^d(OMe)_3$ ligand was at low field (δ = 125.0 ppm) and appeared as a 1:4:1 triplet due to coupling to ^{195}Pt, $^1J(Pt^2P^d) = 4990$ Hz. The presence

Table V. ^{31}P and ^{195}Pt NMR Data for Complexes **5a–d** in CD_2Cl_2 at −90 °C

	5a[b]	5b[c]	5c	5d
$\delta(P^a)$	−35.5	−35.1	−20.0	−25.4
$^1J(PtP^a)$ (Hz)	2280	2240	2400	*a*
$^2J(PtP^a)$ (Hz)	470	500	*a*	*a*
$\delta(P^b)$	−12.3	−13.7	−6.9	−16.2
$^1J(PtP^b)$ (Hz)	2540	2540	2700	*a*
$^2J(PtP^b)$ (Hz)	250	260	*a*	*a*
$^3J(P^bP^b)$ (Hz)	230	240	*a*	*a*
$\delta(P^c)$	−20.6	−20.8	−11.0	−7.9
$^1J(PtP^c)$ (Hz)	3720	3640	3700	3520
$^2J(PtP^c)$ (Hz)	169	180	*a*	*a*
$^3J(P^aP^c)$ (Hz)	190	200	*a*	150
$\delta(P^d)$	125.0	118.2	99.5	−4.0
$^1J(PtP^d)$ (Hz)	4990	4960	6230	3800
$^2J(P^aP^d)$ (Hz)	27	*a*	135	*a*

[a] Not resolved, broad peak. [b] The Pt^1, Pt^3 resonance was not resolved. $\delta(Pt^2)$ = −3242; $^1J(Pt^1Pt^2)$ = 2280 Hz, $^1J(Pt^2H)$ = 1200 Hz, $^1J(Pt^2P^d)$ = 4990 Hz, $^1J(Pt^2P^a)$ = 2280 Hz, $^2J(Pt^2P^c)$ = 170 Hz. [c] $\delta(Pt^2)$ = −3150; $^1J(Pt^1Pt^2)$ = 2200 Hz, $^1J(Pt^2H)$ = 1190 Hz, $^1J(Pt^2P^d)$ = 4960 Hz, $^1J(Pt^2P^a)$ = 2240 Hz.

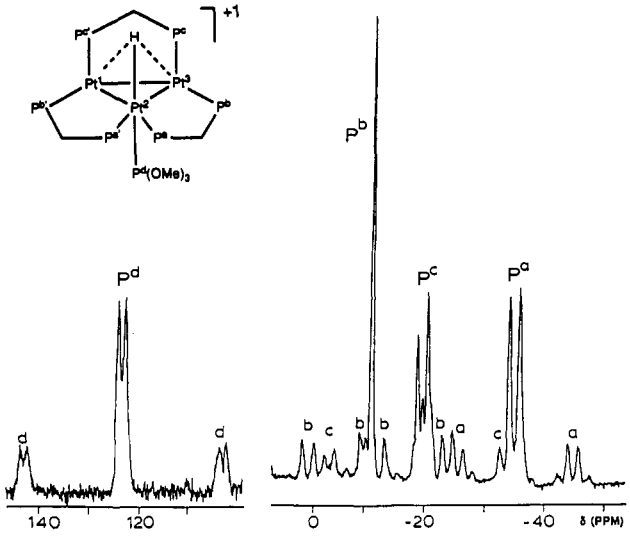

Figure 3. ^1H-coupled ^{31}P NMR spectrum of complex **5a** at −90 °C. Note the doublet splitting of the P^d resonance due to $^2J(P^dH)$.

of a single hydride ligand trans to P^d was indicated by the ^1H-coupled ^{31}P NMR spectrum (Figure 3), which showed an extra doublet splitting due to $^2J(P^dH)$ = 170 Hz.

The hydride signal in the low-temperature ^1H NMR spectrum of **5a** was observed at δ = −0.04 ppm, as a doublet due to coupling to the phosphorus atom of the phosphite ligand [$^2J(P^dH)$ = 170 Hz], and with inner satellites [intensities 1:8:18:8:1; $^1J(Pt^1H)$ = $^1J(Pt^3H)$ = 268 Hz] and outer satellites [intensities ca. 1:4:1; very broad and barely resolved from noise; $^1J(Pt^2H) \simeq 1200$ Hz]. The coupling $^1J(Pt^2H)$ = 1200 Hz was confirmed from the extra well-defined doublet splitting observed in the Pt^2 signal of the ^1H-coupled (compared to the ^1H-decoupled) ^{195}Pt NMR spectrum at −90 °C.

The above spectroscopic data clearly show that the structures in solution are of the type found in the solid state for **5a**. In particular, the phosphine or phosphite ligands adopt a terminal bonding position and the hydride ligand is asymmetrically triply bridged with much stronger bonding to Pt^2 than to Pt^1 or Pt^3. As noted early, the solid-state structure is somewhat less symmetrical than the solution structure deduced by low temperature NMR in that the Pt(1)–Pt(2) and Pt(2)–Pt(3) bond distances are significantly different in the solid.

Fluxionality in Complexes 5. Complexes **5** were fluxional at room temperature. The fluxionality involves migration of the ligand L around the triangular face of the cluster, as shown in eq 2, and established earlier for $[Pt_3(\mu_3\text{-}CO)(\mu\text{-}dppm)_3L]^{2+}$.[10]

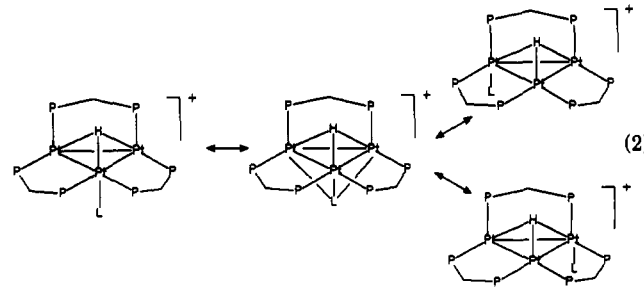

The ^{31}P NMR spectrum of **5a** (Figure 2) at room temperature showed a single broad resonance due to the dppm phosphorus atoms [δ = −21.6, $J_{obs}(PtP)$ = 2980 Hz] and a sharp resonance due to the $P(OMe)_3$ ligand with broad satellites due to $J_{obs}(PtP)$ = 1733 Hz. The calculated value of $J_{obs}(PtP)$ for rapid intramolecular fluxionality in **5a** (eq 2) would be $J_{obs}(PtP^d) \sim {}^1/_3 \times 4990 = 1633$ Hz, in reasonable agreement with the observed value. When free phosphite ligand was present in solution, no exchange between free and complexed $P(OMe)_3$ occurred. This and the observation of $J(PP)$ and $J(PtP)$ coupling for coordinated $P(OMe)_3$ in the fast exchange regime prove that the fluxionality is an intramolecular process.[10]

Further evidence on the nature of fluxionality was obtained from the ^1H NMR spectra. At room temperature the hydride resonance of **5a** still occurred as a doublet with $^2J(P^dH)$ = 170 Hz, due to coupling to the phosphite phosphorus, but an average ^{195}Pt coupling $^1J(PtH)$ = 592 Hz was observed. The calculated value is $J(PtH) = ({}^1/_3 \times 1200) + ({}^2/_3 \times 268) = 579$ Hz, in good agreement. Thus, the hydride appears to be symmetrically triply bridging in the fast fluxionality region, but the coupling $^2J(PH)$ to the phosphite ligand is still maintained. This confirms that the fluxionality does not involve reversible dissociation of either the phosphite or the hydride ligand and so supports the mechanism of eq 2.

Discussion: Bonding in Complexes 5a–d

It has been argued above that complexes **5** contain an asymmetrically triply bridging hydride, with the hydride bound most strongly to the platinum atom with the highest coordination number. Analogous complexes $[Pt_3(\mu_3\text{-}MPPh_3)(\mu\text{-}CO)_3(PPh_3)_3]^+$, (**6**, M = Au; **7**, M = Ag) contain the 44-electron $[Pt_3(\mu\text{-}CO)_3(PPh_3)_4]$ unit, which is isoelectronic with the $[Pt_3(\mu\text{-}dppm)_3\{P(OMe)_3\}]$ unit in **5a**, capped by an MPR_3^+ unit, which is isolobal to H^+ present in **5a**.[23,24] In **6** and **7**, the MPR_3^+ unit was shown crystallographically to be most strongly bound to the platinum atom with the highest coordination number (Table VI). For example, in **6** the strong Au–Pt(2) overlap is reflected in the near linearity of the P–Au–Pt(2) angle [173.5 (1) Å], and the Au–Pt distances [Au–Pt(2) = 2.700 (1) Å, Au–Pt(1) = 2.902 (1) Å and Au–Pt(3) = 2.910 (1) Å].[23] Thus, the similar structures of complexes **2**, **5a**, **6**, and **7** appear to reflect similar bonding modes. Since neither the hydride nor, probably, the MPR_3 ligand has π-acceptor properties, the structures of **5a**, **6**, and **7** cannot result from π-bonding effects of these ligands as had been proposed for **2**. In order to study this problem further, EHMO calculations[25] were carried out for the model compounds $[Pt_3(\mu_3\text{-}H)(PH_3)(\mu\text{-}H_2PCH_2PH_2)_3]^+$ for **2** and $[Pt_3(\mu_3\text{-}CO)(PH_3)(\mu\text{-}H_2PCH_2PH_2)_3]^+$ for **5**, respectively [a calculation with $P(OH)_3$ in place of PH_3 gave a very similar result].

Calculations were first carried out with the complexes in the idealized geometries with symmetrical $Pt_3(\mu_3\text{-}H)$ and $Pt_3(\mu_3$-

(23) Bour, J. J.; Kanters, R. P. F.; Schlebos, P. P. J.; Bos, W.; Bosman, W. P.; Behm, H.; Beurskens, P. T.; Steggerda, J. J. *J. Organomet. Chem.* **1987**, *329*, 405.
(24) Bhaduri, S.; Sharma, K.; Jones, P. G.; Erdbrugger, C. F. *J. Organomet. Chem.* **1987**, *326*, C46.
(25) Summerville, R. H.; Hoffmann, R. *J. Am. Chem. Soc.* **1978**, *98*, 7240.

Table VI. Comparison of Core Distances (Å) in Asymmetric 44e Triplatinum Clusters (Pt^2 Having the Highest Coordination Number)

	2[a]	5a[b]	6[c]	7[d]
Pt^1–Pt^2	2.656 (2)	2.706 (1)	2.702 (1)	2.712 (1)
Pt^2–Pt^3	2.626 (2)	2.635 (1)	2.708 (1)	2.701 (1)
Pt^1–Pt^3	2.636 (2)	2.593 (1)	2.666 (1)	2.674 (1)
Pt^2–X	1.93 (3)		2.700 (1)	2.741 (1)
Pt^1–X	2.16 (3)		2.902 (1)	2.823 (1)
Pt^3–X	2.27 (3)		2.910 (1)	2.915 (1)

[a] X = C(O). [b] X = H. [c] X = Au(PPh_3). [d] X = Ag(PPh_3).

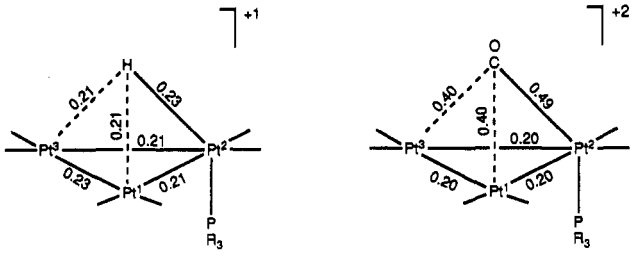

3 4

Figure 4. Computed values of the reduced overlap populations for the PtH, Pt–CO, and Pt–Pt bonds of the complexes $[Pt_3(\mu_3\text{-H})(PH_3)(\mu\text{-}H_2PCH_2PH_2)_3]^+$ (**2**) and $[Pt_3(\mu_3\text{-CO})(PH_3)(\mu\text{-}H_2PCH_2PH_2)_3]^+$. The hydride and carbonyl ligands were in the symmetrically bridging position with d(Pt–H) = 1.85 Å and d(Pt–CO) = 2.16 Å.

CO) units. The computed overlap populations are illustrated in Figure 4. It can be seen that the Pt^2–H overlap [$\rho(Pt^2H)$ = 0.227; $\rho(Pt^2H)/\rho(Pt^1H)$ = 1.09] is greater than the Pt^1–H or Pt^3–H overlap and that the Pt^1–Pt^3 overlap (ρ = 0.232) is greater than the Pt^1–Pt^2 or Pt^2–Pt^3 overlap (ρ = 0.213). Thus, the calculation correctly predicts that the Pt^2H and Pt^1Pt^3 bonds will be the strongest of the PtH and PtPt bonds respectively. Similar data for complex **2** are also shown in Figure 4. It can be seen that the calculation predicts a greater degree of asymmetry in the carbonyl binding [$\rho(Pt^2C)/\rho(Pt^1C)$ = 1.22] but that qualitatively the distortion is predicted to be similar for **2** and **5**. This indicates that the distortion must be due primarily to σ-bonding rather than π-bonding effects of the capping ligand.

Qualitatively, the distortion is most easily understood by considering **5** to be formed by reaction of the neutral cluster $[Pt_3(\mu\text{-dppm})_3(PR_3)]$ with the electrophile H^+, analogous to the actual mode of formation of **6** and **7**. The electrophile will naturally interact most strongly with the most electron-rich center, which is clearly expected to be Pt^2, the platinum atom with the highest coordination number. A correlation diagram illustrating

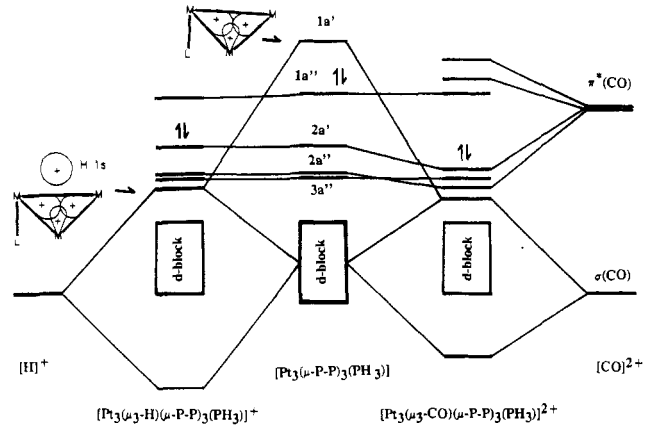

Figure 5. Energy correlation diagrams for the interaction of $[Pt_3(PH_3)(\mu\text{-}H_2PCH_2PH_2)_3]$ with H^+ and CO^{2+}. The stabilization of the 1a′ orbital on interaction with H^+ is illustrated by the orbital diagrams. Because Pt^2 is most electron-rich it interacts most strongly with the proton. The interaction of 1a′ with the empty σ(CO) orbital of CO^{2+} is similar to the interaction with the empty 1s orbital of H^+, which is illustrated.

the bonding interactions is shown in Figure 5. For comparison, this Figure also shows the similar correlation diagram for interaction of $[Pt_3(\mu\text{-dppm})_3(PR_3)]$ with the hypothetical CO^{2+} to form **2**, a process which is chemically fanciful but theoretically instructive. The HOMO for $[Pt_3(\mu\text{-}H_2PCH_2PH_2)_3(PH_3)]$ is calculated to be cluster antibonding (1a″) while the LUMO is the cluster bonding orbital (1a′); the neutral cluster is therefore unlikely to be stable. Addition of the proton stabilizes 1a′ by the process shown in Figure 5 while leaving the other high-lying orbitals unchanged. The result is that in **5** the cluster bonding orbital is occupied, while the antibonding orbital is not, and the cluster is stabilized. CO^{2+} is a stronger electrophile so that the stabilization by the σ-effect is greater and, in addition, the calculation also predicts a weaker π-acceptor bonding which leads to further stabilization (Figure 5). The π-acceptor effect of CO therefore may accentuate the degree of distortion in **2** compared to **5**, but the basic distortion is explicable in terms of σ-bonding only.

Acknowledgment. We thank the NSERC (Canada) for financial support.

Supplementary Material Available: Text giving details of the X-ray structure determination and tables of atomic positional and thermal parameters (Table S1), hydrogen atom positional and thermal parameters (Table S2), complete bond distances and angles (Table S3), selected torsion angles (Table S4), weighted least squares plane (Table S5), and anisotropic thermal parameters (Table S6) (12 pages). Ordering information is given on any current masthead page.